The microtubule-based motor Kar3 and plus end–binding protein Bim1 provide structural support for the anaphase spindle

Melissa K. Gardner,[1] Julian Haase,[2] Karthikeyan Mythreye,[2] Jeffrey N. Molk,[2] MaryBeth Anderson,[2] Ajit P. Joglekar,[2] Eileen T. O'Toole,[3] Mark Winey,[3] E.D. Salmon,[2] David J. Odde,[1] and Kerry Bloom[2]

[1]Department of Biomedical Engineering, University of Minnesota, Minneapolis, MN 55455
[2]Department of Biology, University of North Carolina, Chapel Hill, NC 27599
[3]Molecular, Cellular, and Developmental Biology, University of Colorado at Boulder, Boulder, CO 80309

In budding yeast, the mitotic spindle is comprised of 32 kinetochore microtubules (kMTs) and ~8 interpolar MTs (ipMTs). Upon anaphase onset, kMTs shorten to the pole, whereas ipMTs increase in length. Overlapping MTs are responsible for the maintenance of spindle integrity during anaphase. To dissect the requirements for anaphase spindle stability, we introduced a conditionally functional dicentric chromosome into yeast. When centromeres from the same sister chromatid attach to opposite poles, anaphase spindle elongation is delayed and a DNA breakage-fusion-bridge cycle ensues that is dependent on DNA repair proteins. We find that cell survival after dicentric chromosome activation requires the MT-binding proteins Kar3p, Bim1p, and Ase1p. In their absence, anaphase spindles are prone to collapse and buckle in the presence of a dicentric chromosome. Our analysis reveals the importance of Bim1p in maintaining a stable ipMT overlap zone by promoting polymerization of ipMTs during anaphase, whereas Kar3p contributes to spindle stability by cross-linking spindle MTs.

Introduction

Mitotic chromosome segregation requires the formation of a stable bipolar spindle. Interpolar microtubules (ipMTs) from opposing spindle pole bodies (SPBs) form an organized array by cross-linking with each other (Winey et al., 1995). ipMTs may be cross-linked by MT-based motor proteins and/or MT-associated proteins. This arrangement contributes to the structural stability of the two halves of the mitotic spindle during metaphase and provides the means by which SPBs are rapidly separated from each other during anaphase B. Deletions of the plus end–directed MT-based motor protein *CIN8* or *KIP1* lead to abnormally short metaphase spindles (Saunders et al., 1997), suggesting that these plus end–directed motors generate outwardly directed extensional forces on the SPBs via the sliding of ipMTs against each other. Cells lacking both Cin8p and Kip1p are not viable but deletion of *KAR3* suppresses this lethality, suggesting that the minus end–directed motor Kar3p provides an inward force that opposes the outward force generated by Cin8p and Kip1p (Saunders and Hoyt, 1992). In support of the prediction that Kar3p provides an inwardly directed spindle force, overexpression of Kar3p produces shorter spindles (Saunders et al., 1997). However, in contrast to this prediction, spindles in *kar3*Δ mutants are short (Page and Snyder, 1992; Zeng et al., 1999; Sproul et al., 2005). Thus, the role of Kar3p in the balance of spindle forces that determines mitotic spindle length and stability is unclear.

In addition to Kar3p generating inwardly directed spindle forces, it could be that Kar3p functions passively as an ipMT cross-linker, thus resisting spindle collapse (Hoyt et al., 1993). For example, the MT plus end–binding protein Ase1p acts to bundle MTs and thus stabilize the anaphase spindle (Pellman et al., 1995; Schuyler et al., 2003; Janson et al., 2007). Similarly, Bim1p, the yeast EB1 homologue, may contribute to ipMT interactions through its function at MT plus ends (Tirnauer et al., 1999). It has been difficult to test the function of various MT-binding proteins during mitosis because of the complexity of forces generated between parallel and antiparallel MTs and the forces generated between oppositely oriented sister chromatids.

The structure of the anaphase spindle in yeast provides a unique system to address the function of MT-binding proteins in the maintenance of spindle stability. By anaphase, sister

Correspondence to Kerry Bloom: kerry_bloom@unc.edu

Abbreviations used in this paper: Chr III, chromosome III; ipMT, interpolar MT; kMT; kinetochore MT; MT, microtubule; SPB, spindle pole body.

The online version of this paper contains supplemental material.

The Journal of Cell Biology, Vol. 180, No. 1, January 14, 2008 91–100
http://www.jcb.org/cgi/doi/10.1083/jcb.200710164

chromatids have separated and kinetochore MTs (kMTs) have shortened to the spindle poles (kMTs, ~50 nm in length; Winey et al., 1995). Thus, the ipMTs are responsible for maintaining spindle integrity throughout anaphase.

In this work, we used a conditionally functional dicentric chromosome to test the structural stability of the anaphase spindle. When centromeres from sister chromatids attach to opposite poles, tension across the DNA strand satisfies the spindle checkpoint (Dewar et al., 2004). Cohesin is degraded, anaphase onset ensues, sister centromeres migrate to opposite poles (anaphase A), and sister chromatids segregate. However, segregation of centromeres on sister chromatids of a dicentric chromosome are restrained via their covalent linkage. Anaphase spindle elongation is delayed until the error is resolved. In wild-type cells, resolution is characterized by DNA breakage, with >70% survival. Alternatively, if spindle breakage precedes DNA breakage, the entire chromosome is missegregated. Missegregation of the entire chromosome leads to aneuploidy and subsequent cell death.

Using the conditionally functional dicentric assay, we find that cell survival after dicentric chromosome activation requires the MT-binding proteins Kar3p, Bim1p, and Ase1p. In their absence, anaphase spindles have poor structural stability and therefore collapse and break in the presence of a dicentric chromosome. Our analysis reveals the importance of Bim1p in maintaining a stable ipMT overlap zone by promoting growth of ipMT plus ends during anaphase, whereas Kar3p contributes to spindle stability by acting to cross-link spindle MTs.

Results

Viability in response to activation of a dicentric chromosome requires spindle-associated proteins

Strains with an activated dicentric chromosome that lacked the spindle-associated proteins Bim1p, Kar3p, Cik1p, Ase1p, or Bik1p were 20–300-fold reduced in viability as compared with wild-type cells with an activated dicentric chromosome (Fig. 1, A and B; and Table S1, available at http://www.jcb.org/cgi/content/full/jcb.200710164/DC1). The most severe defect was observed in *bim1*Δ and *kar3*Δ, followed by *bik1*Δ, *cik1*Δ, and *ase1*Δ. The loss of viability in these mutants is comparable to mutants in DNA repair (*rad52*), indicating that an essential function is abrogated in their absence.

Although several of these MT-binding proteins have been implicated in kinetochore function (Tytell and Sorger, 2006), two pieces of evidence argue that kinetochore defects are not the cause of the decreased viability in the presence of a dicentric chromosome. First, our findings with mutations in spindle-associated proteins are different than those previously reported for kinetochore mutants. Specifically, kinetochore mutant cells with activated dicentric chromosomes do not have decreased viability (Fig. 1 B; Doheny et al., 1993; Brock and Bloom, 1994; Mythreye and Bloom, 2003). Second, the MT-associated binding protein Ase1 has no known kinetochore function but is required for ipMT function during anaphase (Pellman et al., 1995; Schuyler et al., 2003).

Dicentric chromosome breakage is reduced in cells lacking these spindle-associated proteins

If the structural integrity of the anaphase spindle is compromised, dicentric chromosome activation may result in spindle breakage and/or failure rather than dicentric chromosome breakage. To test whether dicentric chromosomes break and rearrange in *bim1*Δ mutants, wild-type and *bim1*Δ cells were transformed with the conditionally dicentric minichromosome *pGAL-CEN*^{2}. DNA breakage and rearrangement products can be detected by transformation into bacteria and subsequent gel electrophoresis (Hill and Bloom, 1987). Monocentric rearrangements occurred in 50 out of 50 minichromosomes recovered from wild-type cells (Fig. 2 A, wt), with loss of one of the two centromeres (*CEN3* or *CEN4*). In contrast, ~50% of dicentric minichromosomes recovered from *bim1*Δ cells contained both centromeres (Fig. 2 A, *bim1*Δ, first two lanes, rearrangement products in 23 out of 50; last six lanes, unrearranged 27 out of 50). Thus, the reduced viability of *bim1*Δ mutants is accompanied by an increase in propagation of the intact dicentric chromosome. The appearance of rearrangement products in 23 out of 50 cells indicates that reduced viability in *bim1*Δ mutants is not caused by a deficiency in DNA repair.

To examine the rearrangement frequency of a dicentric chromosome, we introduced *GAL-CEN3* into *HIS4* on chromosome III (Chr III) in wild-type and *bim1*Δ mutants (Brock and Bloom, 1994). In wild-type cells, a 1.1-kb repair product diagnostic of breakage and recombination between *GAL-CEN3* and *CEN3* on Chr III (Hill and Bloom, 1989) was observed within 2.5–5 h after dicentric chromosome activation (Fig. 2 B). The 1.1-kb repair product was not apparent until 12–24 h after switching *bim1*Δ cells to glucose (Fig. 2 B). Quantitative analysis indicated 7.4% of *GAL-CEN3* was intact after wild-type cells were switched to glucose for 30 h, whereas 36% of *GAL-CEN3* remained in *bim1*Δ cells (Fig. 2 C). Intact *GAL-CEN3* was elevated fivefold and the 1.1-kb rearrangement product decreased fourfold in *bim1*Δ cells, which is indicative of reduced chromosome breakage (Fig. 2, C and D). A decrease in the 1.1-kb repair product was also observed in *ase1*Δ and *kar3*Δ cells (Fig. S2, available at http://www.jcb.org/cgi/content/full/jcb.200710164/DC1). These data reveal that dicentric chromosomes are physically stable in *bim1*Δ, *ase1*Δ, and *kar3*Δ mutants.

Dicentric chromosomes missegregate in spindle-associated protein mutants

To determine if the loss of viability after dicentric chromosome activation in *bim1*Δ mutants reflects missegregation of the intact dicentric chromosome, we used the LacO–LacI–GFP system to visualize the dicentric chromosome in live cells (Straight et al., 1997; Thrower and Bloom, 2001). The LacO coding sequence was integrated between the two centromeres on Chr III at *LEU2*. LacI fused to GFP was expressed to image the dicentric chromosome. In wild-type cells with an activated dicentric chromosome, chromosome spots at *LEU2* remain as a single focus of fluorescence between the spindle poles until sister chromatids separate in anaphase and two spots are visible (Fig. 3, A and B). However, in *bim1*Δ cells the dicentric chromosome is

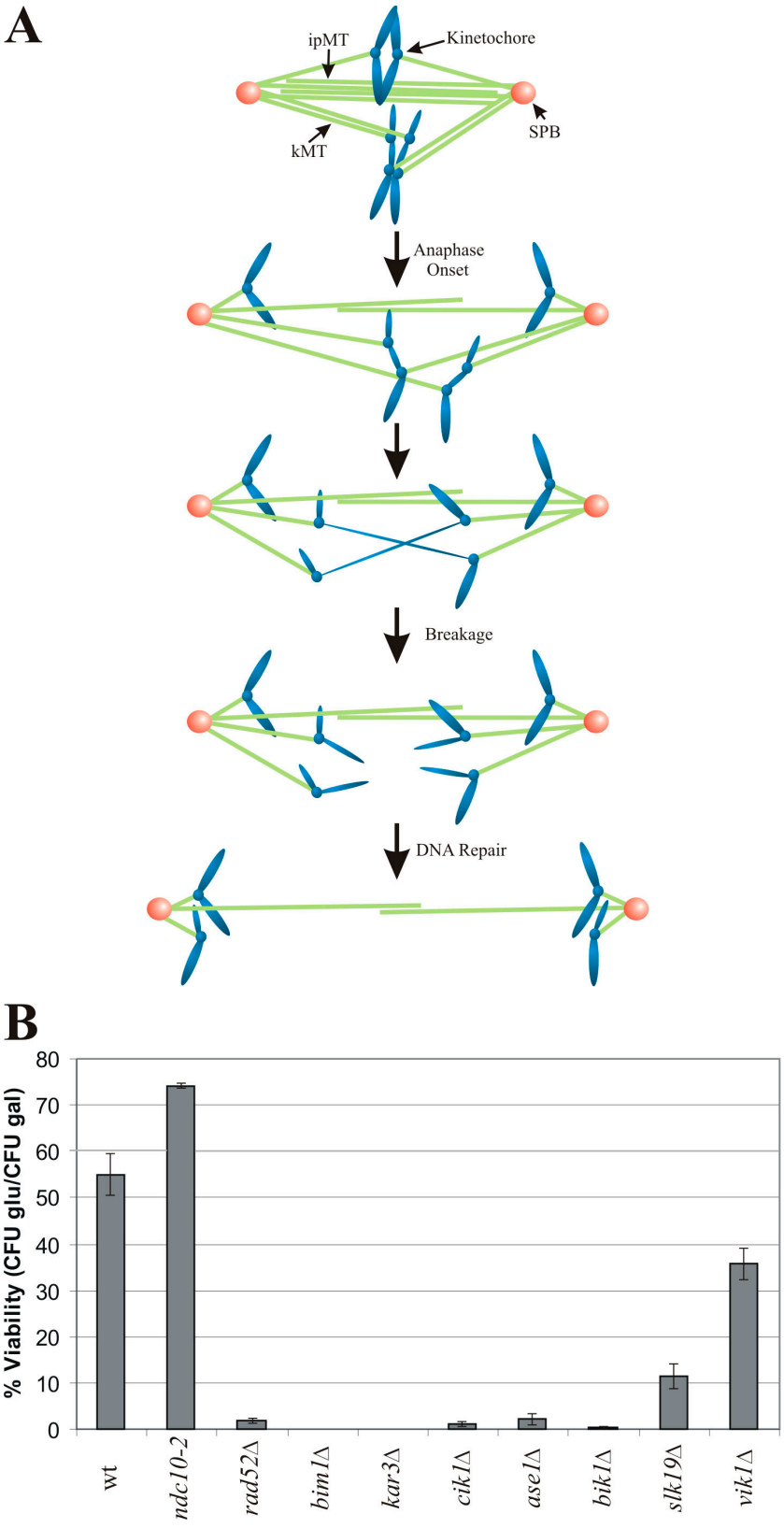

Figure 1. **Dicentric chromosome activation results in decreased viability in MT plus end–binding mutants.** (A) Schematic of dicentric chromosome activation in wild-type cells. In ~50% of cells with an activated dicentric chromosome, the kinetochores will orient toward opposite SPBs. After anaphase onset, the bioriented dicentric chromosome will stretch between both SPBs, resulting in a midanaphase pause. To resume anaphase, the dicentric chromosome breaks and the DNA lesion is repaired to generate a monocentric derivative (blue, chromosomes; green, MTs; orange, SPBs). (B) Histogram of the viability of cells with an activated dicentric chromosome. Centromeres on the dicentric chromosome were in the direct orientation, except for *rad52Δ* cells, which, along with *ndc10-2*, have been reported previously (Brock and Bloom, 1994; Mythreye and Bloom, 2003). Error bars are the standard deviation for each determination. Data for both orientations can be found in Table S1 (available at http://www.jcb.org/cgi/content/full/jcb.200710164/DC1).

found proximal to one SPB in 48.5% of cells (vs. 6% in wild-type cells; Fig. 3 A), whereas 17.5% cells had >2 Chr III spots (vs. 2% in wild-type cells; Fig. 3, A and B). Thus, the frequency of missegregation of the intact dicentric chromosome is highly elevated in *bim1Δ* mutants.

Spindle-associated protein mutants have unstable spindles in the presence of a dicentric chromosome

We imaged MTs (GFP-Tub1p) in mitotic spindles to assess the structural stability of wild-type and mutant cells in the presence of

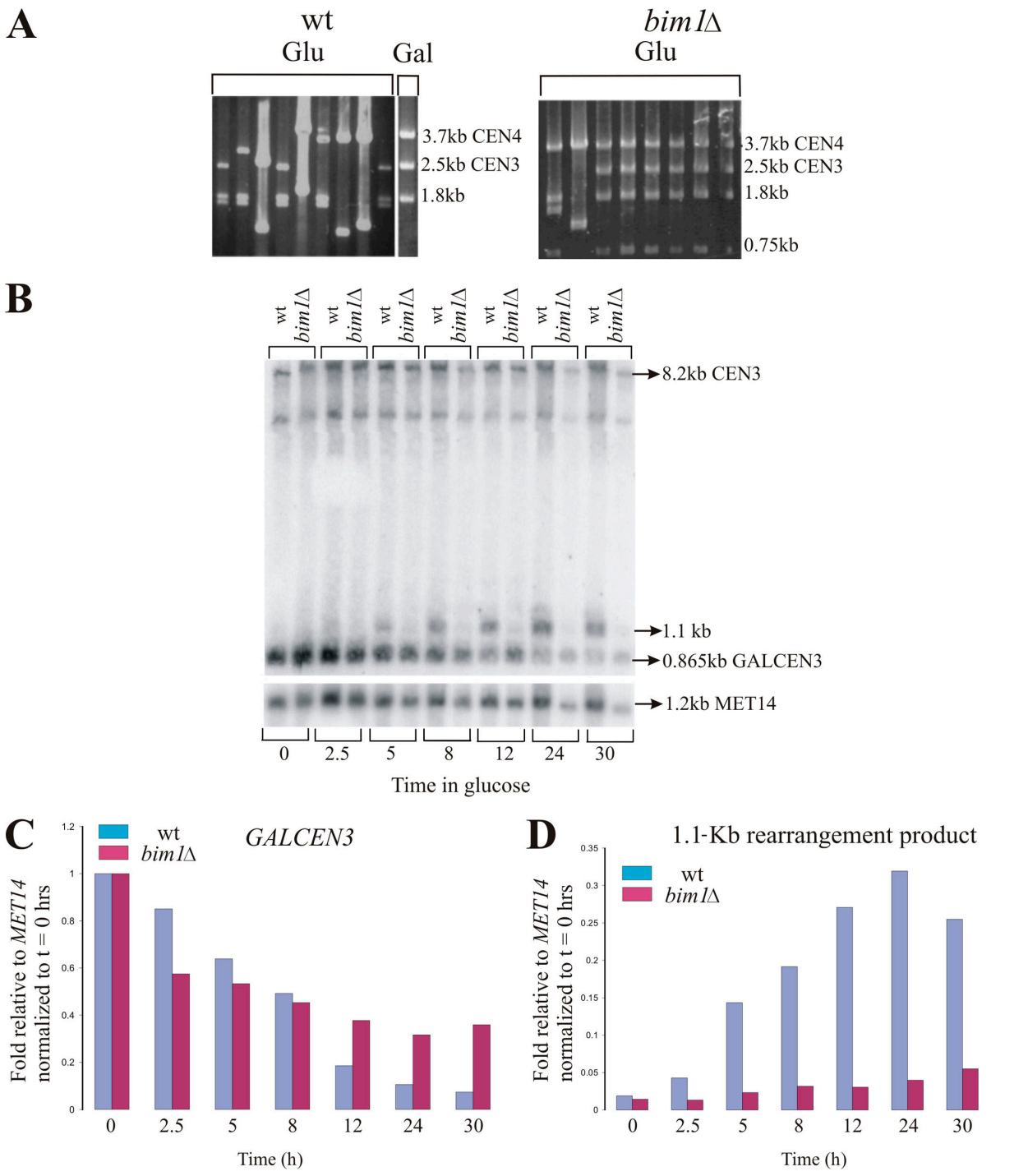

Figure 2. ***bim1Δ* suppresses dicentric chromosome breakage.** (A) Restriction analysis of dicentric plasmid *pGAL-CEN*[2] DNA (Hill and Bloom, 1989) recovered from wild-type or *bim1*Δ cells maintained on galactose or glucose. Plasmid DNA derived from wild-type and *bim1*Δ cells was digested as previously described (Hill and Bloom, 1989). In wild-type cells, 0 out of 50 cells had both centromeres intact after plasmid recovery and analysis. 27 out of 50 dicentric plasmids derived from *bim1*Δ cells had both centromeres intact. Molecular masses of DNA fragments after restriction digestion of the unrearranged plasmid are indicated to the right of each gel. CEN4 and CEN3 indicate the fragments containing the centromere fragment from Chr IV or III, respectively. (B) Time course for monocentric derivatives generated by recombination between the two centromeres on Chr III. Wild-type and *bim1*Δ cells were cultured and the time course was performed as previously described (Brock and Bloom, 1994). Time (in hours) indicates the time points after activating the dicentric chromosome (switch to glucose). At each time point, the chromosomal DNA was prepared and analyzed by Southern analysis (see Materials and methods). The Southern blot was also probed for *MET14* that served as a loading control. Molecular masses for each of the respective fragments are indicated to the right of each gel (kb). (C) Histogram of the percentage of radioactive *GAL-CEN3* relative to *MET14* over the time course for wild-type and *bim1*Δ cells as determined by ImageQuant analysis. There was a 13.5-fold decrease in the *GAL-CEN3* band in wild-type cells but only a 2.8-fold decrease in *bim1*Δ. (D) Histogram of the percentage of radioactive 1.1-kb rearrangement product relative to *MET14* over the time course for wild-type and *bim1*Δ cells as determined by ImageQuant analysis. There was a 13.6-fold increase in the 1.1-kb rearrangement product in wild-type cells but only a 3.8-fold increase in *bim1*Δ cells.

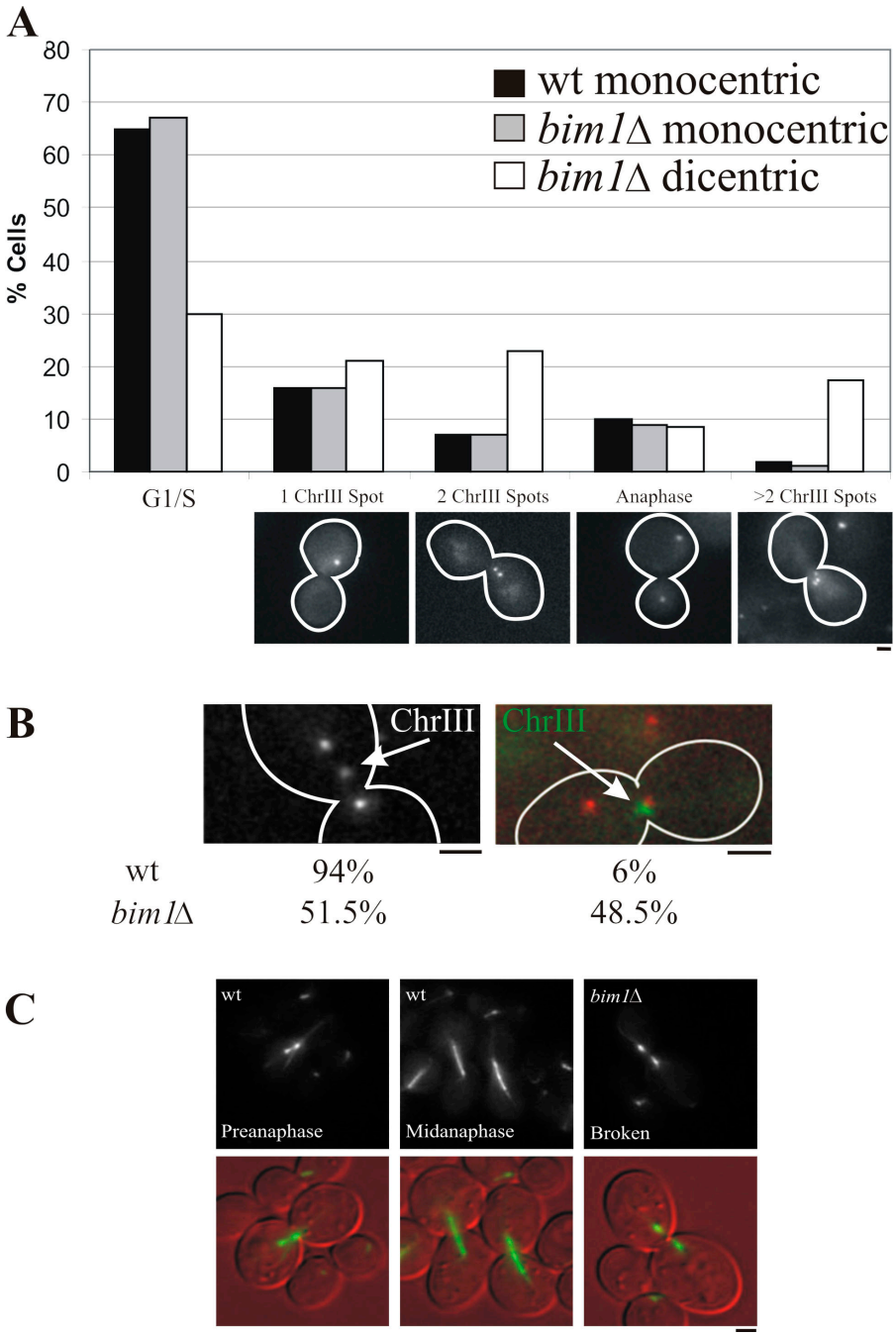

Figure 3. **The dicentric chromosome is mis-segregated in *bim1*Δ cells.** (A) Histogram of Chr III segregation in wild-type, *bim1*Δ monocentrics, and *bim1*Δ dicentrics from cells expressing LacI–GFP with LacO integrated at *LEU2* on Chr III. Unbudded or small budded cells were classified as G1/S. Medium to large budded cells were scored for one Chr III spot, two Chr III spots, two separated Chr III spots in anaphase, or less than two Chr III spots. Wild-type monocentrics were maintained on glucose (n = 91 cells); *bim1*Δ monocentrics were grown on galactose (n = 139); and *bim1*Δ dicentrics were cultured on glucose (n = 169). Bar, 2 μm. (B) Activated dicentric Chr III behavior relative to SPBs. Arrows marks the position of Chr III. Both cell types have LacO integrated at Chr III and expressed LacI–GFP. Wild-type SPBs were marked with Spc72p-GFP. *bim1*Δ cell SPBs were marked with Spc29p-RFP. Population images were taken 3 h after switching cells to glucose. Dicentric Chr III position relative to the SPB was determined by measuring the distance of the Chr III spot from the SPB and the distance between the two SPBs. Wild-type cells (n = 97) have 94% of Chr III spots within the central one third of the distance between SPBs. Only 51.5% of *bim1*Δ cells (n = 105) have the Chr III spot in the central one third of the spindle. Bars, 2 μm. (C) Spindle morphology in wild-type and *bim1*Δ cells with activated dicentric chromosomes. Top, GFP-Tub1p images; bottom, overlay of GFP-Tub1p (green) with differential interference contrast image (red). In wild-type cells, spindles are in preanaphase or arrest in midanaphase with continuous GFP-Tub1p fluorescence. In 38% of *bim1*Δ cells with activated dicentric chromosomes that entered anaphase, the GFP-Tub1p fluorescence was not continuous, which suggests that spindles had broken. Bar, 2 μm.

an activated dicentric chromosome. In >95% of wild-type cells with an activated dicentric chromosome, GFP-Tub1p was continuous along the length of the spindle in both preanaphase and anaphase (Fig. 3 C; n = 57 cells). However, 38% of mitotic *bim1*Δ cells displayed discontinuous GFP-Tub1p fluorescence that appeared as two foci (Fig. 3 C; n = 166 cells). The two GFP-Tub1p fluorescent foci could separate >5 μm before moving back together (unpublished data). Thus, when the anaphase spindle is constrained by a dicentric chromosome bridge the *bim1*Δ ipMTs cannot maintain a continuous overlapping array. The gap in GFP-Tub1p could result from spindle destabilization, possibly related to a change in ipMT length (Tirnauer et al., 1999) or cross-linking defects. In either case, ipMT function is required in anaphase for cells to resolve the dicentric chromosome into monocentric derivatives. In contrast, weakening of mitotic spindle structural stability via loss of ipMT function favors chromosome missegregation and/or spindle breakage rather than dicentric chromosome breakage and rearrangement.

ipMT-associated tubulin polymer is reduced in *bim1*Δ cells but not in *kar3*Δ cells

If both Bim1p and Kar3p contribute to spindle stability, as is predicted by the dicentric assay, then the loss of these proteins should result in a quantifiable defect in anaphase spindle morphology. To test this prediction we examined the distribution of GFP-Tub1p in anaphase spindles of wild-type and mutant cells

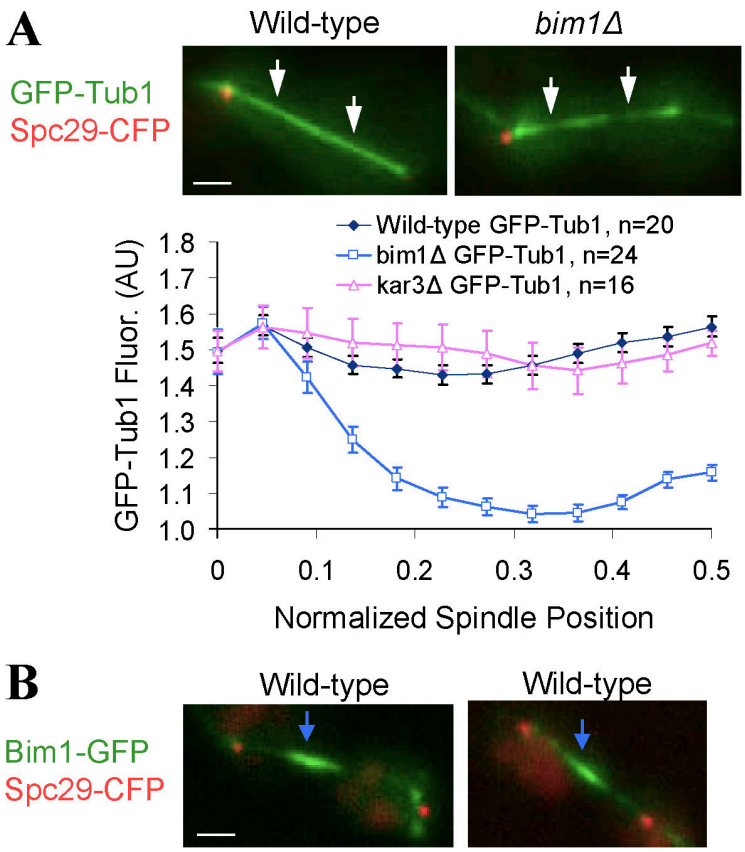

Figure 4. **Anaphase tubulin polymer is reduced in *bim1*Δ cells.** (A) GFP-Tub1p fluorescence is nearly uniform along the length of wild-type anaphase spindles (top left; white arrows show approximate minimum intensity location), suggesting that ipMTs are nearly as long as the spindle itself (spindle length 5.04 ± 0.93 µm [mean ± SD]). In contrast, GFP-Tub1p fluorescence has decreased intensity in *bim1*Δ cells (top right; white arrows show approximate minimum intensity location; note comparison to wild-type spindle in similar location), suggesting that ipMTs have reduced length as compared with wild-type spindles (spindle length 5.15 ± 1.21 µm). Quantification of GFP-Tub1 fluorescence by normalized spindle position shows reduced GFP-Tub1p fluorescence in *bim1*Δ anaphase spindles as compared with wild-type spindles (bottom, spindle position normalized to total spindle length). Error bars represent SEM. Bar, 1,000 nm. (B) Bim1-GFP (green) is localized within the spindle midzone (blue arrows; spindle lengths 4.66 ± 0.97 µm; for quantification see Fig. S1 A, available at http://www.jcb.org/cgi/content/full/jcb.200710164/DC1). Bar, 1,000 nm.

using quantitative microscopy and model convolution. In wild-type cells, there is a uniform distribution of GFP-Tub1p fluorescence along the entire length of the anaphase spindle (Fig. 4 A). Anaphase GFP-Tub1 fluorescence levels in *kar3*Δ mutants are comparable to those in wild-type spindles (Fig. 4 A), suggesting that reduced spindle stability upon *KAR3* deletion is not caused by improper length regulation of ipMTs. In contrast, there is a sharp drop in GFP-Tub1p fluorescence in *bim1*Δ anaphase spindles (Fig. 4 A). These results suggest that the tubulin polymer associated with ipMTs during anaphase may be reduced in *bim1*Δ mutants as compared with wild-type spindles. In contrast, another spindle defect may prevail in the absence of Kar3p.

Bim1-GFP is concentrated at the spindle midzone in anaphase (Fig. 4 B and Fig. S1 A, available at http://www.jcb.org/cgi/content/full/jcb.200710164/DC1), suggesting that Bim1p is bound near to ipMT plus ends during anaphase. Bim1p promotes growth of astral MTs in G1 (Tirnauer et al., 1999) and is likely to have a similar mechanism of action when bound to ipMT plus ends in anaphase.

During anaphase, bim1Δ mutant ipMTs are shorter than wild-type ipMTs

To quantify ipMT length, we used electron tomography to reconstruct MT length distributions in wild-type anaphase spindles. By normalizing all MT lengths to the individual spindle lengths of two anaphase spindles, we found one class of abundant, short MTs. These MTs exhibit an exponential length distribution, with their plus ends clustered near to the spindle poles (Fig. 5 A, bottom left; mean ± SD, 7 ± 7.7% of spindle length [absolute length, 151 ± 213 nm]; $n = 64$ MTs; probability of fit to exponential model (p-value) = 0.59 [see Materials and methods for calculation procedure]). Based on the position of kinetochores at this stage of anaphase, this polymer class represents kMTs. Longer ipMT lengths were also exponentially distributed but extended the length of the spindle, with plus ends clustered near the opposite SPB from their origin (Fig. 5 A, bottom right; mean ± SD is 78 ± 15% of spindle length [absolute length, 1,555 ± 447 nm]; $n = 14$ MTs; $P = 0.27$ for fit to exponential [see Materials and methods for p-value calculation procedure]).

To use model convolution to statistically compare tubulin distributions in different populations, we sampled the exponential fit curves from the tomograms (Fig. 5 A) to generate simulated GFP-Tub1p distributions of anaphase spindles. By convolving the experimentally observed microscope point-spread function with the simulated GFP-Tub1p distributions (Gardner et al., 2007; see Materials and methods), we could directly compare simulated images (Fig. 5 B, bottom) to GFP-Tub1p experimental images (Fig. 5 B, top). Simulated images based on electron tomography data qualitatively match experimental fluorescence images (Fig. 5 B, graph; $P = 0.07$). Thus, the exponential wild-type ipMT length distribution obtained via quantitative analysis of electron tomography data is a reasonable approximation of wild-type anaphase spindles (Fig. 5 B, animation).

The theoretical length distribution of anaphase spindle MTs that most closely reproduced the experimentally observed GFP-Tub1p fluorescence distribution in the absence of Bim1p is shown in Fig. 5 C. The best fit to experimental data could be obtained using a Gaussian ipMT length distribution with mean ± SD of

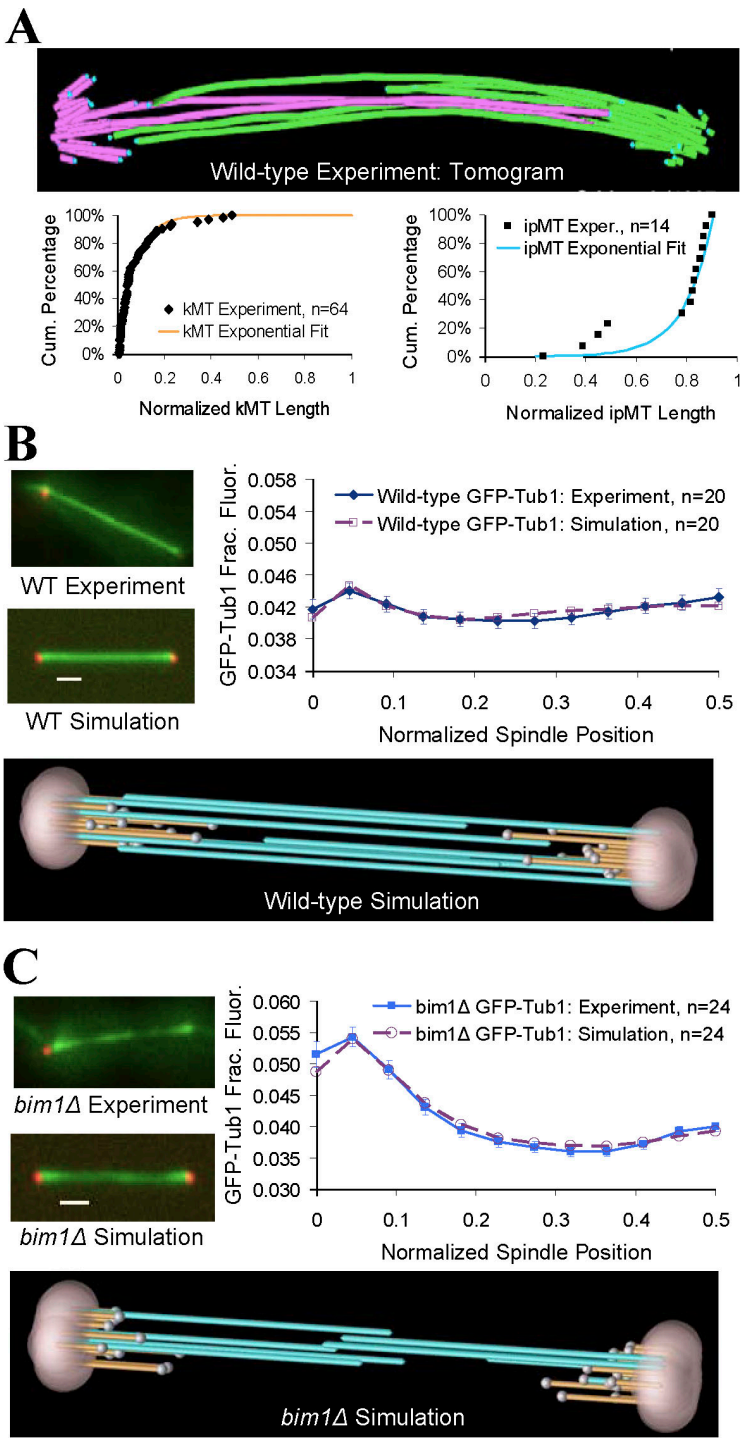

Figure 5. **Model convolution analysis suggests that the midzone overlap zone in *bim1*Δ anaphase spindles is reduced compared with wild-type spindles.** (A) 3D model of a typical wild-type anaphase spindle using electron tomography (top). Individual MTs from each spindle pole (magenta and green, respectively) were traced as model contours in a tomographic volume containing a complete spindle. The 32 shortest MTs were classified as kMTs in each of two spindles, and normalized cumulative length distribution is plotted (bottom left). The remaining longer MTs were then classified as ipMTs and plotted separately (bottom right). Both kMT and ipMT lengths followed exponential distributions, with kMTs short and near to each SPB, and ipMTs longer, running nearly the entire length of the spindle (orange and cyan lines; see Materials and methods). (B) Exponential models derived from the wild-type tomogram analysis were sampled to produce simulated GFP-Tub1 fluorescence images via model convolution (left). Images simulated using wild-type kMT and ipMT tomogram length distribution models qualitatively reproduce experimental fluorescence images (right). A typical animation is shown at the bottom (orange, kMTs; cyan, ipMTs). Error bars represent SEM. Bar, 1,000 nm. (C) The ipMT length distribution was then modified in simulation to reproduce the experimentally observed distribution of GFP-Tub1 in *bim1*Δ anaphase spindles (left and right). The best-fit model predicts that ipMT length is reduced, resulting in a substantially shorter ipMT midzone overlap zone (animation, bottom). Error bars represent SEM. Bar, 1,000 nm.

52 ± 7% of spindle length (Fig. 5 C; P = 0.06). Thus, we predict that the ipMT plus ends in *bim1*Δ mutants are located very near to the spindle equator, which results in a significant decrease in the antiparallel ipMT overlap zone as compared with wild-type spindles (Fig. 5 C, animation, compare with Fig. 5 B, animation).

The role of Bim1p in regulating MT length is consistent with previous observations (Tirnauer et al., 1999). The decrease in overlap of antiparallel MTs in *bim1*Δ mutants would reduce the number of productive binding sites available for the kinesin-5 motors Cin8p and Kip1p, preventing *bim1*Δ spindles from achieving the outwardly directed force threshold that is required to break dicentric chromosomes. Interestingly, cell viability after activation with a dicentric chromosome was increased ~12-fold in a *bim1*Δ/*kip3*Δ double mutant as compared with *bim1* mutants with an activated dicentric chromosome (*bim1*Δ/*kip3*Δ dicentric viability, 6.8 ± 0.73%; n = 4 trials). This result suggests that an increase in ipMT length (in the absence of the MT depolymerizing motor Kip3p) is sufficient to stabilize the anaphase spindle, thus increasing viability after activation of a dicentric chromosome.

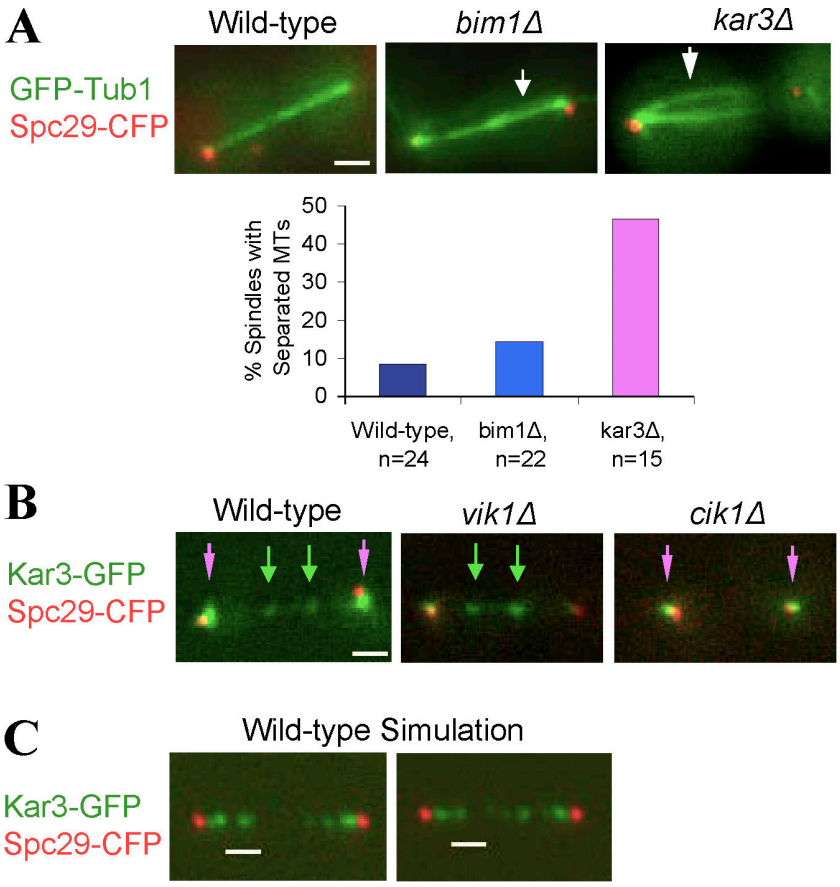

Figure 6. **ipMT bundling is reduced in *kar3Δ* mutant anaphase spindles.** (A) ipMT bundling is compared in wild-type, *bim1Δ*, and *kar3Δ* anaphase spindles by examining the splaying of MTs within the spindle. Splaying of ipMTs in *kar3Δ* spindles is readily apparent (right, white arrow) as compared with well-bundled wild-type and *bim1Δ* spindles (white arrow; *kar3Δ* spindle length 5.49 ± 1.04 μm [mean ± SD]; wild-type and *bim1Δ* spindle lengths as in Fig. 4). Bar, 1,000 nm. (B) Kar3-GFP is localized near to the SPBs (magenta arrows) as well as in punctate spots within the spindle (left, green arrows). Analysis of Kar3-GFP localization in *vik1Δ* and *cik1Δ* spindles suggests that the Kar3p–Cik1p complex is localized both near to the SPBs (magenta arrows) and within the spindle (middle, green arrows), whereas the Kar3p–Vik1p complex is localized near to the SPBs (right, magenta arrows). Bar, 1,000 nm. (C) Modeling results are consistent with the prediction that the Kar3p–Cik1p complex is localized at the plus ends of anaphase MTs. Bars, 1,000 nm.

Kar3p regulates bundling of ipMTs during anaphase

Because deletion of *KAR3* did not have a significant effect on anaphase spindle tubulin polymer (Fig. 4), we predicted that another spindle defect, such as the proper bundling of ipMTs, may prevail in the absence of Kar3p. To test this prediction, we examined mutant spindle morphology in *kar3Δ* mutants expressing GFP-Tub1p. As shown in Fig. 6 A, 47% of *kar3Δ* spindles showed splaying of MTs in anaphase. Thus, ipMTs are poorly bundled in *kar3Δ* mutants as compared with wild-type spindles (8% MT separation). Disrupting the organization of ipMTs may also disturb proper antiparallel cross-linking of Cin8p and Kip1p and suggests that Kar3p is required for efficient attachment of the kinesin-5 motors Cin8p and Kip1p to oppositely oriented ipMTs. Therefore, deletion of *KAR3* results in reduced outwardly directed spindle forces as mediated by kinesin-5 motors, even though Kar3p itself may act to antagonize Cin8p/Kip1p function in wild-type spindles.

Kar3p is known to interact with either Cik1p or Vik1p light chains in vivo and in vitro (Manning et al., 1999; Sproul et al., 2005; Allingham et al., 2007). Because *cik1Δ* mutants have low cell viability in response to activation of a dicentric chromosome, we predicted that the Kar3p–Cik1p complex may regulate spindle integrity via the ipMT bundling mechanism, as shown in Fig. 6 A, and thus localize near to ipMT plus ends in the anaphase spindle. Indeed, although Kar3-GFP is localized at the SPB in wild-type anaphase spindles it is also present in punctuate locations within the spindle (Fig. 6 B, left). To assess Kar3p–Cik1p binding exclusively, we examined Kar3-GFP localization in *vik1Δ* spindles (Fig. 6 B, middle and Fig. S1 B). Here, there is reduced fluorescence of Kar3-GFP near to the SPB, with increased fluorescence in punctuate spots near putative ipMT plus ends. Simulations in which fluorescent proteins are distributed at the plus ends of MTs also resulted in punctuate spots along the length of the spindle (Fig. 6 C). In contrast, Kar3-GFP that is complexed with Vik1p (in *cik1Δ* cells) is focused at the SPBs with little fluorescence along the length of the spindle (Fig. 6 B, right; and Fig. S1 B). These results demonstrate that the light chains Cik1p and Vik1p differentially regulate the localization and function of Kar3p to either the ipMT plus ends (Cik1p) or spindle poles (Vik1p). In addition, our results suggest that Kar3p–Cik1p regulates ipMT bundling along the length of the spindle and that poor ipMT bundling is the dominant mechanism for low cell viability in response to activation of a dicentric chromosome in *kar3Δ* mutants.

Discussion

There are two pathways required for cell survival in the presence of a dicentric chromosome. Dicentric chromosomes are physically unstable and undergo a breakage-fusion-bridge cycle that is required for cell survival (Fig. 1 A). We found a second pathway required for cell survival, which is the maintenance of spindle integrity. If the spindle is compromised, spindle breakage results in chromosome loss and the subsequent loss of cell viability.

Using the activated dicentric chromosome assay, we find that Bim1p and Kar3p both contribute to structural stability of

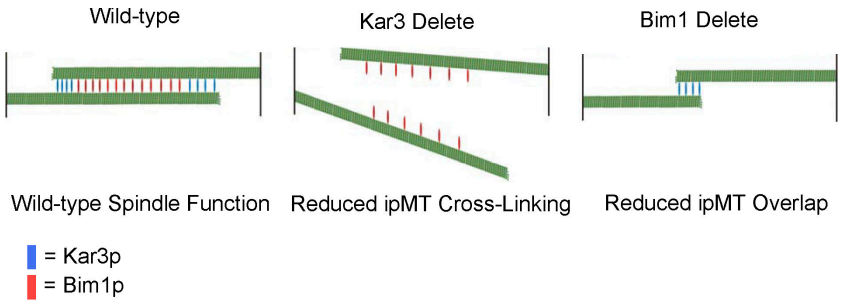

Figure 7. **A model for the distinct roles of Kar3p and Bim1p in mechanically stabilizing the anaphase spindle.** In wild-type spindles (left), Kar3p and Bim1p cooperate to maintain an ipMT midzone overlap zone of sufficient length and width. In *kar3*Δ mutants, ipMTs are splayed apart (middle) compromising the robust structural stability of the anaphase spindle. In contrast, *bim1*Δ mutants are properly bundled but have shorter ipMTs (right), reducing the length of the antiparallel midzone overlap zone. Both improper bundling and a reduced midzone overlap zone likely frustrate proper attachment and cross-linking of the motor proteins that provide outwardly directed spindle forces during anaphase (Cin8p and Kip1p).

the anaphase spindle. Interestingly, the mechanisms by which these proteins contribute to stability are distinct from each other but appear to be of similar importance (Fig. 1 B). Specifically, deletion of *BIM1* results in shorter ipMT lengths, which reduces the size of the anaphase antiparallel overlap zone (Fig. 7, right). The ipMT overlap zone is necessary for efficient antiparallel binding of the kinesin-5 motors Cin8p and Kip1p, so reducing its length likely has a direct effect on the ability of the kinesin-5 motors to provide the outwardly directed forces that are required to stabilize the elongating anaphase spindle.

In contrast, deletion of *KAR3* does not have a significant effect on the level of anaphase tubulin polymer (Fig. 4). Rather, *kar3*Δ mutants show splaying of anaphase ipMTs, likely because of improper ipMT bundling as mediated by Kar3p–Cik1p complexes at the plus ends of ipMTs (Fig. 6). The differential localization of Kar3-GFP in *cik1*Δ mutants and *vik1*Δ mutants (Fig. 6 B) is consistent with the difference in activated dicentric lethality between the mutants (Fig. 1 B), suggesting that spindle-bound Kar3p acts to promote ipMT bundling. Similar to the *bim1*Δ mutants, poor ipMT bundling in *kar3*Δ mutants also likely prevents proper antiparallel binding of the kinesin-5 motors and therefore results in reduced outwardly directed spindle forces (Fig. 7, middle). This effect explains the long-standing enigma of how spindle lengths could be shorter in *kar3*Δ mutants even though Kar3p could act to resist outwardly directed spindle forces when ipMTs are properly bundled.

These results highlight the importance of the spindle midzone structure in maintaining anaphase spindle integrity. An important future effort will involve mechanistically linking the spindle localization of Kar3p and Bim1p to their specific functions within the anaphase spindle.

Materials and methods

Media, growth conditions, and strain construction

Strains and plasmids used in this study are listed in Table S2 (available at http://www.jcb.org/cgi/content/full/jcb.200710164/DC1). Media and strains, including gene deletions and GFP fusions, were prepared as described previously (Mythreye and Bloom, 2003; Molk et al., 2004). Deletions of *BIM1* were confirmed by PCR amplification and by sensitivity to 15 μg/ml of benomyl. Strains were maintained at 25°C, except for some wild-type and *bim1*Δ cells carrying dicentric chromosomes that were grown at 32°C. *kar3*Δ cells expressing GFP fusion proteins were maintained at 25°C overnight and switched to 32°C for 2–3 h before imaging. For imaging chromosome spots, cells were grown in galactose or glucose for two to four generations before analysis. Cells with a conditional dicentric chromosome were grown in YCAT-Gal (galactose; monocentric) overnight at 25°C to midlogarithmic phase and diluted into YPD (glucose; dicentric) to analyze dicentric chromosome behavior. Approximately 1,000 cells were diluted in water and plated on YPG or YPD for viability assays. Plates were incubated at 25°C for up to 10 d before colonies were scored. Wild-type and *bim1*Δ cells were transformed with *pGAL-CEN*[2] on galactose and single transformants were grown for 8–10 generations in either galactose or glucose before plasmid DNA was isolated and transformed into *Escherichia coli* for analysis.

Dicentric chromosome breakage analysis: Southern blotting and PCR

Time course experiments on glucose and Southern blotting were performed as previously described (Brock and Bloom, 1994). Wild-type and cells with conditional dicentric chromosomes were grown overnight in 50 ml YCAT-Gal or YPG media and switched to fresh YPD at the start of the experiment. At time points, yeast was collected by centrifugation and genomic DNA was prepared. For Southern blotting, the genomic DNA was digested with BamHI and, after transfer of the DNA, the blot was probed with [^{32}P]*GAL-CEN* that was generated by PCR with Klenow polymerase. The blot was stripped and reprobed for [^{32}P]*MET14* as a control. Band intensity was measured using ImageQuant. For PCR assays, 1 μl of genomic DNA was added to a 50-μl reaction (200 nM deoxyribonucleotide triphosphates, 4% DMSO, and 400 nM of primers) that was cycled as follows: 98°C, 1 min; melting temperature 95°C, 1 min; annealing temperature 60°C, 1 min; extension temperature 72°C, 2 min for 27 cycles; and final extension temperature 72°C, 5 min. 5 μl of each PCR reaction was loaded on a 1% agarose gel and stained for 15 min in 0.02% ethidium bromide before analysis.

Fluorescence image acquisition and data analysis

Wide-field (Molk et al., 2004) and confocal (Maddox et al., 2003) images were obtained as previously detailed. The microscope used for wide-field imaging was a TE2000E stand (Eclipse; Nikon) with a 100 NA 1.4 objective (PlanApo) with a camera (Orca ER; Hamamatsu). Images were acquired at room temperature with MetaMorph imaging software (MDS Analytical Technologies). Differential interference contrast image exposure times were for 150–200 ms and epifluorescence exposure times were 300–400 ms. LacI–GFP expression was induced as described previously (Thrower and Bloom, 2001). Images were processed as previously detailed (Molk et al., 2004). To quantify the dicentric Chr III missegregation events, cells were grown overnight in glucose media and induced for LacI–GFP expression for 2 h and five-plane Z series of the population were acquired. The percentage of mitotic cells in the population was also recorded at this time. Fluorescence intensity measurements by spindle position were performed as previously described (Gardner et al., 2005). All measurements were exported to Excel (Microsoft) for further analysis.

Electron tomography

Cells were prepared for electron microscopy using methods previously described (Winey et al., 1995). In brief, log-phase cultures were collected by vacuum filtration and high-pressure frozen using a high-pressure freezer (BalTech). The frozen cells were freeze substituted in 1% OsO_4 and 0.1% uranyl acetate in acetone and embedded in epon resin. Serial 250-nm-thick sections were collected onto formvar-coated slot grids and stained with lead citrate and uranyl acetate.

Dual axis tomography was performed as described previously (O'Toole et al., 2002). 15 nm of colloidal gold was affixed to each surface of the sections to serve as fiducial markers for tomography. The specimens were imaged using a microscope (TECNAI F30; FEI) operated at 300 kV. Images were captured every 1° over a ±60° range at a pixel size of 1 nm around two orthogonal axes. The serial tilted views were then aligned and dual axis tomograms, computed using the IMOD software package (Kremer et al., 1996; Mastronarde, 1997). Tomograms were computed from adjacent serial sections to reconstruct complete mitotic spindles.

In total, we reconstructed two wild-type anaphase spindles. Individual MTs were modeled from the tomographic volumes and a projection of the 3D model was then displayed to study its 3D geometry. MT lengths were extracted from the model contour data using the program IMODINFO.

Modeling of MT length distributions

MT length distributions obtained from electron tomography were fit to exponential models as follows. It was assumed that the 32 shortest MTs in each spindle were kMTs. The cumulative distribution of kMT lengths were then fit to an exponential distribution according to $F(L) = 1 - e^{L/Lmean}$, where F(L) is the cumulative distribution function for MT length, L is MT length normalized to spindle length, and L_{mean} is the mean normalized MT length for the sample. All measured MTs longer than the 32 shortest in each spindle were assumed to be ipMTs. The cumulative distribution of ipMT lengths were fit to an exponential distribution according to $F(L) = e^{-\{(L\,max\,-\,L)/(L\,max\,-\,Lmean)\}}$, where L_{max} is the maximum observed normalized MT length, which is 0.905. This correction takes into account an experimentally observed ipMT plus end–exclusion zone near to the SPBs, possibly caused by entropic or steric exclusion originating from the high density of kMTs near to the poles.

A bootstrap method was used for calculating fit probability of experimental data to exponential models, as previously described (Sprague et al., 2003; Gardner et al., 2007). Here, a set of 100 simulated sum-of-squares error (SSE_{sim}) values were calculated by comparing each simulated MT length distribution curve (generated via sampling from the exponential fit curve) to the mean curve over all 100 simulations. The experimental SSE value (SSE_{exp}) was then calculated by comparing the experimental data to the mean simulation curve. The SSE_{exp} was ranked in the list of 100 simulated SSE_{sim} values to calculate the probability of fit (p-value).

Model-convolution simulations

Model convolution of simulated fluorescence distributions was completed by convolving the experimentally observed microscope point spread function with the simulated distribution of fluorescent proteins, as previously described (Sprague et al., 2003; Gardner et al., 2007). Calculation of p-values for fit of simulated model-convolution images to experimental images was completed as previously described (Sprague et al., 2003; Gardner et al., 2007).

Online supplemental material

Table S1 lists dicentric viability in plus end–binding proteins. Table S2 lists the *Saccharomyces cerevisiae* strains used in this study. Fig. S1 shows quantification of Kar3-GFP and Bim1-GFP fluorescence localization in anaphase spindles. Fig. S2 shows data showing the formation of repair products after dicentric activation in mutant and wild-type cells. Online supplemental material is available at http://www.jcb.org/cgi/content/full/jcb.200710164/DC1.

We thank David Bouck, Jay Gatlin, Erin McCarthy, and members of the Bloom and Salmon laboratories for advice, assistance, and critical readings of the manuscript.

This work was funded by the National Institutes of Health grants GM-32238 (K. Bloom), GM-071522 (D.J. Odde), GM-24364 (E.D. Salmon), and GM-60678 (E.D. Salmon) and the National Center for Research Resources of the National Institutes of Health grant RR-00592 to A. Hoenger (E.T. O'Toole). M.K. Gardner was supported by the National Institutes of Health (EB005568).

Submitted: 24 October 2007
Accepted: 10 December 2007

References

Allingham, J.S., L.R. Sproul, I. Rayment, and S.P. Gilbert. 2007. Vik1 modulates microtubule-Kar3 interactions through a motor domain that lacks an active site. *Cell*. 128:1161–1172.

Brock, J.A., and K. Bloom. 1994. A chromosome breakage assay to monitor mitotic forces in budding yeast. *J. Cell Sci.* 107:891–902.

Dewar, H., K. Tanaka, K. Nasmyth, and T.U. Tanaka. 2004. Tension between two kinetochores suffices for their bi-orientation on the mitotic spindle. *Nature*. 428:93–97.

Doheny, K.F., P.K. Sorger, A.A. Hyman, S. Tugendreich, F. Spencer, and P. Hieter. 1993. Identification of essential components of the *S. cerevisiae* kinetochore. *Cell*. 73:761–774.

Gardner, M.K., C.G. Pearson, B.L. Sprague, T.R. Zarzar, K. Bloom, E.D. Salmon, and D.J. Odde. 2005. Tension-dependent regulation of microtubule dynamics at kinetochores can explain metaphase congression in yeast. *Mol. Biol. Cell*. 16:3764–3775.

Gardner, M.K., D.J. Odde, and K. Bloom. 2007. Hypothesis testing via integrated computer modeling and digital fluorescence microscopy. *Methods*. 41:232–237.

Hill, A., and K. Bloom. 1987. Genetic manipulation of centromere function. *Mol. Cell. Biol.* 7:2397–2405.

Hill, A., and K. Bloom. 1989. Acquisition and processing of a conditional dicentric chromosome in *Saccharomyces cerevisiae*. *Mol. Cell. Biol.* 9:1368–1370.

Hoyt, M.A., L. He, L. Totis, and W.S. Saunders. 1993. Loss of function of *Saccharomyces cerevisiae* kinesin-related CIN8 and KIP1 is suppressed by KAR3 motor domain mutations. *Genetics*. 135:35–44.

Janson, M.E., R. Loughlin, I. Loiodice, C. Fu, D. Brunner, F.J. Nedelec, and P.T. Tran. 2007. Crosslinkers and motors organize dynamic microtubules to form stable bipolar arrays in fission yeast. *Cell*. 128:357–368.

Kremer, J.R., D.N. Mastronarde, and J.R. McIntosh. 1996. Computer visualization of three-dimensional image data using IMOD. *J. Struct. Biol.* 116:71–76.

Maddox, P., A. Straight, P. Coughlin, T.J. Mitchison, and E.D. Salmon. 2003. Direct observation of microtubule dynamics at kinetochores in *Xenopus* extract spindles: implications for spindle mechanics. *J. Cell Biol.* 162:377–382.

Manning, B.D., J.G. Barrett, J.A. Wallace, H. Granok, and M. Snyder. 1999. Differential regulation of the Kar3p kinesin-related protein by two associated proteins, Cik1p and Vik1p. *J. Cell Biol.* 144:1219–1233.

Mastronarde, D.N. 1997. Dual-axis tomography: an approach with alignment methods that preserve resolution. *J. Struct. Biol.* 120:343–352.

Molk, J.N., S.C. Schuyler, J.Y. Liu, J.G. Evans, E.D. Salmon, D. Pellman, and K. Bloom. 2004. The differential roles of budding yeast Tem1p, Cdc15p, and Bub2p protein dynamics in mitotic exit. *Mol. Biol. Cell*. 15:1519–1532.

Mythreye, K., and K.S. Bloom. 2003. Differential kinetochore protein requirements for establishment versus propagation of centromere activity in *Saccharomyces cerevisiae*. *J. Cell Biol.* 160:833–843.

O'Toole, E.T., M. Winey, J.R. McIntosh, and D.N. Mastronarde. 2002. Electron tomography of yeast cells. *Methods Enzymol.* 351:81–95.

Page, B.D., and M. Snyder. 1992. CIK1: a developmentally regulated spindle pole body-associated protein important for microtubule functions in *Saccharomyces cerevisiae*. *Genes Dev.* 6:1414–1429.

Pellman, D., M. Bagget, H. Tu, and G.R. Fink. 1995. Two microtubule-associated proteins required for anaphase spindle movement in *Saccharomyces cerevisiae*. *J. Cell Biol.* 130:1373–1385.

Saunders, W.S., and M.A. Hoyt. 1992. Kinesin-related proteins required for structural integrity of the mitotic spindle. *Cell*. 70:451–458.

Saunders, W., V. Lengyel, and M.A. Hoyt. 1997. Mitotic spindle function in *Saccharomyces cerevisiae* requires a balance between different types of kinesin-related motors. *Mol. Biol. Cell*. 8:1025–1033.

Schuyler, S.C., J.Y. Liu, and D. Pellman. 2003. The molecular function of Ase1p: evidence for a MAP-dependent midzone-specific spindle matrix. *J. Cell Biol.* 160:517–528.

Sprague, B.L., C.G. Pearson, P.S. Maddox, K.S. Bloom, E.D. Salmon, and D.J. Odde. 2003. Mechanisms of microtubule-based kinetochore positioning in the yeast metaphase spindle. *Biophys. J.* 84:3529–3546.

Sproul, L.R., D.J. Anderson, A.T. Mackey, W.S. Saunders, and S.P. Gilbert. 2005. Cik1 targets the minus-end kinesin depolymerase kar3 to microtubule plus ends. *Curr. Biol.* 15:1420–1427.

Straight, A.F., W.F. Marshall, and A.W. Murray. 1997. Mitosis in living budding yeast: anaphase A but no metaphase plate. *Science*. 277:574–578.

Thrower, D.A., and K. Bloom. 2001. Dicentric chromosome stretching during anaphase reveals roles of Sir2/Ku in chromatin compaction in budding yeast. *Mol. Biol. Cell*. 12:2800–2812.

Tirnauer, J.S., E.O. O'Toole, L. Berrueta, B.E. Bierer, and D. Pellman. 1999. Yeast Bim1p promotes the G1-specific dynamics of microtubules. *J. Cell Biol.* 145:993–1007.

Tytell, J.D., and P.K. Sorger. 2006. Analysis of kinesin motor function at budding yeast kinetochores. *J. Cell Biol.* 172:861–874.

Winey, M., C.L. Mamay, E.T. O'Toole, D.N. Mastronarde, T.H. Giddings Jr., K.L. McDonald, and J.R. McIntosh. 1995. Three-dimensional ultrastructural analysis of the *Saccharomyces cerevisiae* mitotic spindle. *J. Cell Biol.* 129:1601–1615.

Zeng, X., J.A. Kahana, P.A. Silver, M.K. Morphew, J.R. McIntosh, I.T. Fitch, J. Carbon, and W.S. Saunders. 1999. Slk19p is a centromere protein that functions to stabilize mitotic spindles. *J. Cell Biol.* 146:415–425.